The 14th International Topical Meeting on Nuclear Reactor Thermalhydraulics, NURETH-14
Toronto, Ontario, Canada, September 25-30, 2011

NURETH14-525

APPLICATION OF VECTOR FINITE VOLUME METHOD FOR ELECTROMAGNETIC FLOW SIMULATION

T. Takata[1], R. Murashige[1], T. Matsumoto[1] and A. Yamaguchi[1]
[1] Osaka University, Suita, Osaka, Japan

Abstract

A vector finite volume method (VFVM) has been developed for an electromagnetic flow analysis. In the VFVM, the governing equations of magnetic flux density and electric field intensity are solved separately so as to reduce the computational cost caused by an iterative procedure that is required to satisfy the solenoidal condition. In the present paper, a suppression of temperature fluctuation of liquid sodium after a T-junction has also been investigated with a simplified two dimensional numerical analysis by adding an obstacle (turbulence promoter) or a magnetic field after the junction.

Introduction

Liquid sodium, used as a coolant of fast reactor, is an electromagnetic fluid and its flow structure can be controlled by the Lorentz force, *e.g.* a magnetic pumping system. One of concerns in a cooling system of sodium cooled fast reactor is a thermal fatigue problem [1] due to a coolant mixture of different temperature in a piping system. When a coolant of different temperature meets at a T-junction as shown in Figure 1, a temperature fluctuation will develop downstream due to a turbulent mixing [2]. As a result, the thermal fatigue may happen on the piping system when the temperature fluctuation is propagated upon the pipe inner surface.

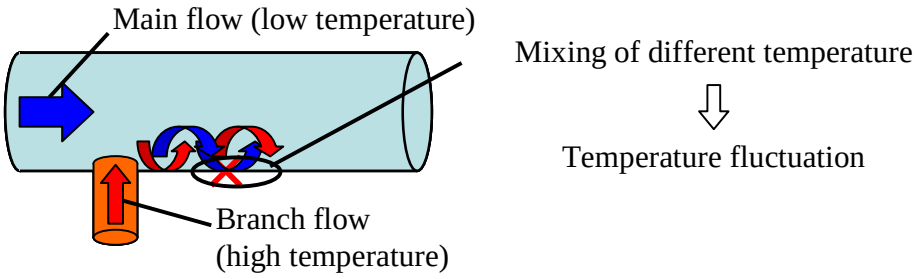

Figure 1 Schematic of temperature mixing after T-junction

A change of flow structure in the mixing region is one of effective manners to reduce the temperature fluctuation. For instance, Tanaka et al. proposed a turbulence promoter to accelerate the turbulent mixing by putting it after the junction [3]. The flow structure of liquid sodium can also be affected by adding a magnetic field. In general, a turbulent flow will weaken due to the Lorentz force and thus the temperature mixing will be suppressed. At the same time, the temperature fluctuation can also weaken although the mixing region will be enlarged. Hence, it is

possible that the characteristic of the temperature fluctuation is changed by adding magnetic field onto liquid sodium.

Since liquid sodium is invisible and an experimental research work is costly, a numerical simulation is useful and helpful for investigation of flow structure. With regard to the numerical simulation of the T-junction, the Large Eddy Simulation (LES) is being applied currently as a turbulent model because an instantaneous turbulent flow structure and its transient affect the temperature fluctuation significantly [1].

As concerns an electromagnetic field simulation, one must solve the governing equations of a magnetic flux and an electric field simultaneously under the solenoidal condition, in which a divergence of the magnetic flux diminishes ($\mathrm{div}\,\mathbf{B}=0$). As a result, an iterative manner is used to solve the electromagnetic field. The application of the LES to an industrial problem requires a large computational cost. Thus it is said that the coupling of the LES and the electromagnetic field and the application to an industrial problem are still challenges.

For the purpose of reducing the computational cost, the authors have been developing a vector finite volume method (VFVM) for an electromagnetic flow field simulation [4], [5]. In the present paper, a simplified two dimensional numerical simulation has been carried out to investigate the applicability of the VFVM coupled with the LES and the influence of the Lorentz force to the temperature fluctuation.

1. Vector finite volume method

1.1 Governing equations and discretization

The governing equations of electromagnetic field consist of Maxwell equations of electromagnetism and Ohm's law as:

$$\mathrm{rot}\,\mathbf{H}=\mathbf{j}+\frac{\partial \mathbf{D}}{\partial t}, \tag{1}$$

$$\mathrm{div}\,\mathbf{B}=0, \tag{2}$$

$$\mathrm{rot}\,\mathbf{E}+\frac{\partial \mathbf{B}}{\partial t}=0, \tag{3}$$

$$\mathbf{j}=\sigma\{\mathbf{E}+\mathbf{u}\otimes\mathbf{B}-\beta(\mathbf{j}\otimes\mathbf{B})\}. \tag{4}$$

Where, **H**, **j**, **D**, **B** and **E** are the Vector forms of magnetic field intensity, current density, electric flux density, magnetic flux density and electric field intensity, respectively. σ and β are the electric conductivity and the Hall constant. $\otimes$ indicates cross product. Then the Lorentz force and the Joule heat are obtained in the following.

$$\mathbf{F}_L = \left(\frac{1}{\mu_m} \mathrm{rot}\,\mathbf{B} \right) \otimes \mathbf{B} \,, \tag{5}$$

$$Q_J = \frac{|\mathbf{j}|^2}{\sigma} \,. \tag{6}$$

Here μ_m is the magnetic permeability.

When electromagnetically isotropy and homogeneity are assumed in a tiny control volume, the magnetic flux is obtained as:

$$\mathbf{B} = \mu_m \mathbf{H} \,. \tag{7}$$

Furthermore, considering no displacement and electric convection currents, Eqs. (1) and (4) are reduced in the following.

$$\mathrm{rot}\,\mathbf{H} = \mathbf{j} \,, \tag{8}$$

$$\mathbf{j} = \sigma(\mathbf{E} + \mathbf{u} \otimes \mathbf{B}) \,. \tag{9}$$

In general, the induction equation is obtained by substituting Eqs. (7)-(9) into Eq. (3) as:

$$\frac{\partial \mathbf{B}}{\partial t} = \mathrm{rot}(\mathbf{u} \times \mathbf{B}) + \frac{1}{\sigma \mu_m} \nabla^2 \mathbf{B} \,.$$

or (10)

$$\frac{\partial \mathbf{B}}{\partial t} = \nabla \cdot (\mathbf{u} \otimes \mathbf{B} - \mathbf{B} \otimes \mathbf{u}) + \frac{1}{\sigma \mu_m} \nabla^2 \mathbf{B} \,.$$

It is carefully noted that the solenoidal condition (Eq. (2)) is not a sufficient condition but a necessary condition in Eq. (10). Hence, an iterative solution is required when one solves Eq. (10) so as to satisfy the solenoidal condition simultaneously.

In the VFVM, the electric field intensity (**E**) and the magnetic flux density (**B**) are solved separately. By substituting Eqs. (7) and (9) into Eq. (8), the electric field intensity is written as:

$$\mathbf{E} = \frac{1}{\sigma \mu_m} \mathrm{rot}\mathbf{B} - \mathbf{u} \otimes \mathbf{B}. \tag{11}$$

The magnetic flux density at subsequent time step is calculated from Eqs. (3) and (11) as;

$$\frac{\partial \mathbf{B}}{\partial t} = \frac{\mathbf{B}^{n+1} - \mathbf{B}^n}{\Delta t} = -\mathrm{rot}\,\mathbf{E}, \tag{12}$$

here superscript n and n+1 mean the current and the subsequent time step respectively. When one multiplies the divergence operator ($\nabla \cdot$) into Eq. (12), the following equation is obtained.

$$\nabla \cdot \mathbf{B}^{n+1} - \nabla \cdot \mathbf{B}^{n} = -\Delta t \nabla \cdot (\mathrm{rot}\,\mathbf{E}) \,. \tag{13}$$

The right hand side of Eq. (13) must be zero mathematically. In the VFVM, the staggered layout of the magnetic flux density and the electric field intensity is applied to achieve it numerically as shown in Figure 2. The magnetic flux density vector is located on the center of each surface (black arrow), while the electric field intensity vector is defined at the center of each side. Therefore, the electric field intensity vector is canceled each other during the divergence operation (see upper right side of the control volume in Figure 2) and thus the right side of Eq. (13) diminishes numerically. As a result, Eq. (13) is rewritten as:

$$\nabla \cdot \mathbf{B}^{n+1} = \nabla \cdot \mathbf{B}^{n} \,. \tag{14}$$

Accordingly the solenoidal condition will satisfy absolutely when it is achieved at an initial condition ($\nabla \cdot \mathbf{B}^{n=0} = 0$). Hence the magnetic field intensity can be updated non-iteratively.

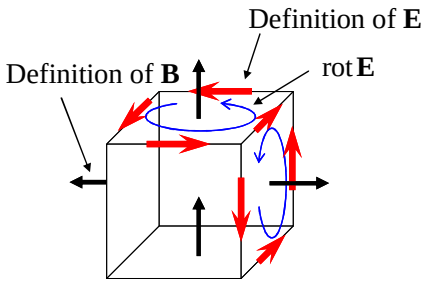

Figure 2 Staggered layout in control volume

1.2 Boundary condition

In the VFVM, the electric field intensity (**E**) is required at a boundary as well as the magnetic flux density. A given value is applied in an input deck as concerns the magnetic flux density, while the electric filed intensity at the boundary is calculated using Eq. (11). As a result, the boundary magnetic flux density must be modified based on Eq. (12) so as to satisfy the solenoidal condition. From the viewpoint of numerical simulation, it is desirable that the magnetic flux density is kept to be constant during each time step once it is given from the input deck. Therefore, the concept of the corrector is introduced and defined in each boundary surface as shown in Figure 3.

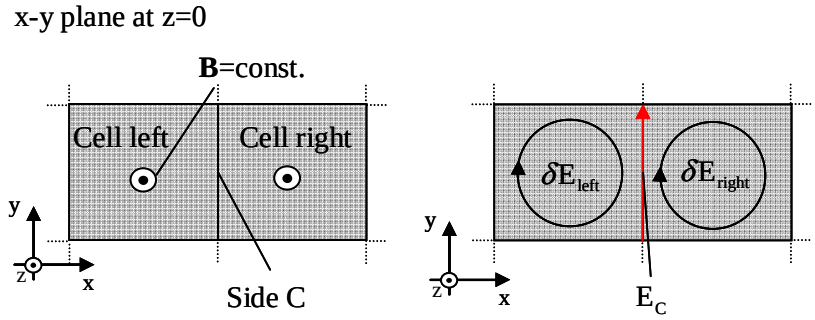

Figure 3 Schematic of electric intensity field corrector

Using the corrector, the electric field intensity on each side is updated as:

$$\mathrm{E_C} = \mathrm{E_C^*} + (\delta \mathrm{E_{right}} - \delta \mathrm{E_{left}}) \,. \tag{15}$$

Here superscript * means the predictor that is calculated from Eq. (11). The corrector is solved under a condition where the magnetic flux field does not change (rot**E**=0) at the boundary. It is mentioned that a matrix solution is required in this process. Hence the iterative manner is still necessary in the VFVM. However, the matrix size becomes small rather than the existing iterative methods because it depends only on the number of boundary surfaces. It is also mentioned that the physical meaning of the corrector is an external force which keeps the boundary condition (magnetic flux field) constant during the time step.

2. Coupling of VFVM with LES simulation

The Lorentz force (Eq. (5)) and the Joule heat (Eq. (6)) is added in governing equations of momentum and energy of the LES simulation [6] as:

$$\bar{\rho}\frac{\partial \bar{\mathbf{u}}}{\partial t} + \nabla \cdot \overline{\rho \mathbf{u}\mathbf{u}} = -\nabla \bar{p} + \frac{\partial}{\partial x_k}\left[(\bar{\mu} + \bar{\rho}\nu_t)\frac{\partial \bar{\mathbf{u}}}{\partial x_k} \right] + (\bar{\rho} - \rho_0)\mathbf{g} + \bar{\mathbf{F}}_L \,, \tag{16}$$

$$\frac{\partial \bar{\rho}\bar{h}}{\partial t} + \nabla \cdot \bar{\rho}\bar{h}\mathbf{u} = \frac{\partial}{\partial x_k}\left[(\bar{\lambda} + \bar{\rho}\overline{Cp}\frac{\nu_t}{Pr_t})\frac{\partial \bar{T}}{\partial x_k} \right] + \bar{Q}_J \,. \tag{17}$$

Here, ρ, t and **u** mean the density, time and velocity vector respectively. p and μ are the pressure and the molecular viscosity. ν_t is the sub-grid scale (SGS) eddy viscosity. x_k and **g** are the k-th coordinate the gravity vector. h, T, λ, Cp and Pr_t indicate the enthalpy, temperature, thermal conductivity, specific heat and turbulent Prandtl number respectively. Q_J means the jule heat (Eq. (6)). Overbar($\bar{\cdot}$) indicate the ensemble average of the SGS. In the present study, a top-hat filter (2nd central differential scheme in advective term) and the standard Smagorinsky model is applied.

As seen in Eq. (10), the reciprocal product of the electric conductivity and the magnetic permeability behaves as a diffusivity of the magnetic flux density. Since liquid sodium has a low magnetic permeability (it is almost equivalent to the space permeability), a much smaller time step is necessary for a stable computation in the electromagnetic filed analysis rather than that in the thermal hydraulic analysis (the LES) in terms of the Courant-Friendrichs-Lewy (CFL) condition. Hence the fractional time step method is applied for the coupling.

In each time step of the computation, the electromagnetic field, the Lorentz force and the Joule heat is updated successively with the smaller time step where the velocity field is kept to be constant. Then the temperature field is updated based on the time averaged Joule heat and the current velocity field. Lastly, the velocity field is updated based on the time averaged Lorentz force. No parallelized programming has been applied for simplicity in the present study.

3. Application to thermal hydraulics analysis of thermal fatigue problem

A numerical analysis of a temperature mixing phenomenon after a T-junction has been carried out in order to investigate an applicability of the present method and an influence of applied magnetic flux on the mixing phenomenon by comparing with a turbulence promoter. In the present study, two dimensional analyses are applied for simplicity (Taking into account the update of the electric field intensity at the boundary, it can be said that 2.5 dimensional analyses are applied.).

3.1 Analytical condition

Figure 4 shows the analytical domain. The T-junction consists of a main pipe (D_m, ϕ40mm) and a branch pipe (D_b, ϕ12mm) taking into account the previous research work [3]. The liquid sodium is assumed as a working fluid and the mean velocities and the temperatures are set to 3.9m/s and 340ºC for the main pipe and 1.0m/s and 430ºC for the branch pipe, which correspond to approximately 4.7×10^5 and 3.6×10^4 of the Reynolds number based on the diameter, respectively.

The analytical domain is segmented into 230(x)×56(y) for the main pipe and 12(x)×40(y) for the branch pipe as shown in Figure 5. The wall is treated as a non-slip and adiabatic condition. The Spalding type wall function is applied to obtain the wall shear stress [7]. In the LES simulation, the standard Smagorinsky (Cs = 0.1) is applied. It is mentioned that a three dimensional analysis must be required for a quantitative investigation. Here a qualitative investigation of the applicability and the influence has been carried out considering a computational cost.

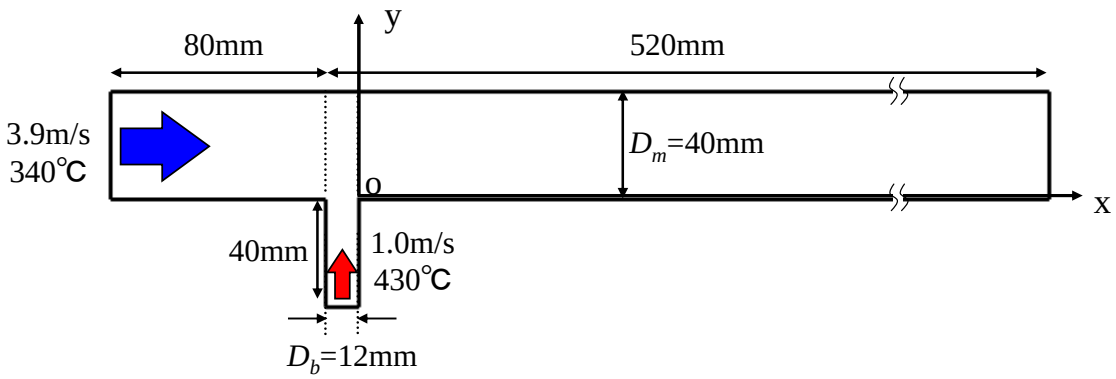

Figure 4 Analytical domain

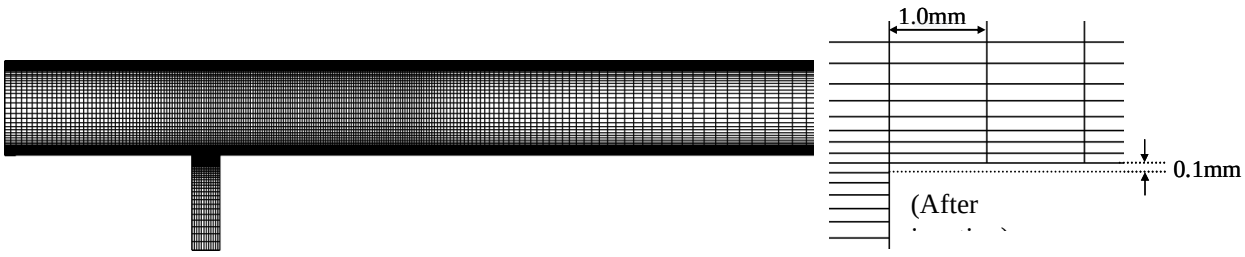

Figure 5 Mesh arrangement

In the analysis, an influence on temperature mixing is investigated by putting a turbulence promoter (Figure 6(a)) and an applied magnetic flux density after the junction (Figure 6(b)). The influence of the Lorentz force on a fluid structure can be represented based on the Hartmann number (*Ha*) and the Reynolds number (*Re*) as:

$$N = \frac{Ha^2}{Re}, \tag{18}$$

which means the proportion of the Lorentz force to the inertial force (*N* is called as an interaction parameter or Stuart number). The magnitude of the magnetic flux density is also chosen as a sensitivity parameter. Table 1 summarizes the analytical cases. In each computation, the time step is set to 4.0×10^{-6}s for thermal hydraulics analysis. In the coupling between the thermal hydraulics and the electromagnetic analyses, a fractional time step of approximately 1.0×10^{-7}s is used for the electromagnetic analysis. As concerns the statistical properties, an average per 1s is applied after a quasi steady state is achieved.

Table 1 Analytical cases

	Installation	Magnetic flux density [T]	*Re* [-] main/branch	*Ha* [-]	*N* [-]
Case 1	-	-	4.7×10^5 / 3.6×10^4	-	-
Case 2	Promoter	-		-	-
Case 3a	Magnetic	0.1		511	0.55
Case 3b	Magnetic	0.2		1022	2.19

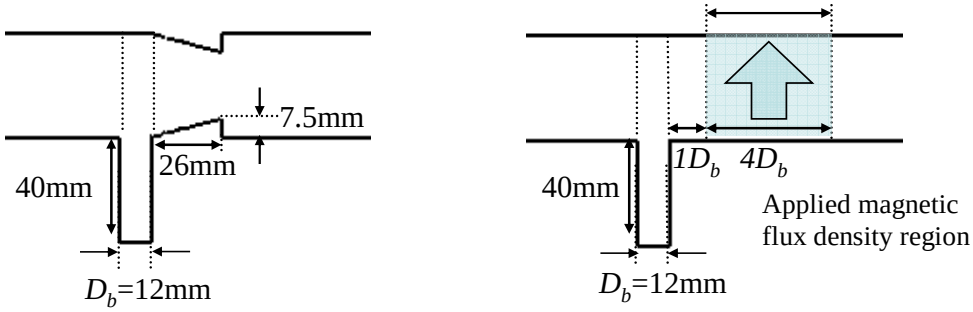

(a) Turbulence promoter (b) Applied magnetic flux density

Figure 6 Additional installations for temperature mixing mitigation

3.2 Results and discussion

Figures 7 and 8 show the instantaneous and the average temperature distributions, respectively. In the present analysis, the branch flow is not fast so that the temperature mixing is investigated along to the bottom side of the main pipe.

As shown in Figure 7(a), a large scale vortex is generated after the T-junction in Case 1 where no additional installation is taken into consideration. Thus the temperature mixing is accelerated and the high temperature region disappears as it goes downstream (Figure 8(a)). When the turbulence

promoter is installed (Case 2), the vortex is enlarged and shifted to the center of the main pipe (Figure 7(b)). Consequently, the high temperature region vanishes rapidly comparing with Case 1 as shown in Figure 8(b).

On the contrary, no large scale vortex is investigated when the magnetic flux density is applied as seen in Figures 7(c) and (d). This is attributed to the fact that the flow structure inside the applied magnetic field is constrained to flatten by the Lorentz force. As a result, the turbulent mixing weakens and the branch flow is pushed out toward the bottom of the main pipe. Accordingly, the high temperature region exists downstream in Case 3a and 3b rather than Case 1 and 2 (see Figure 8). With regard to the magnitude of the applied magnetic field, the flow structure is affected more as the interaction parameter (N) increases (0.55 -> 2.19). However, it seems that no large difference is investigated in terms of the instantaneous and average temperature distributions.

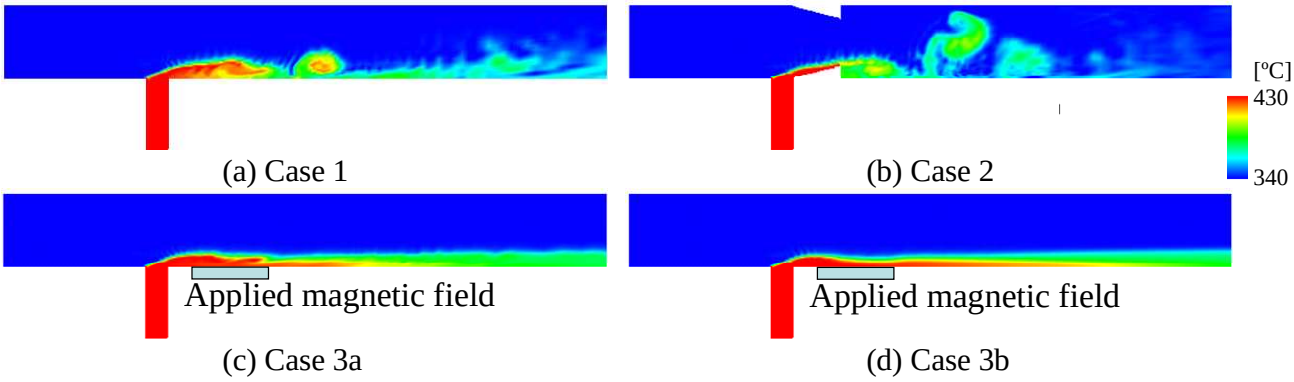

(a) Case 1 (b) Case 2

(c) Case 3a (d) Case 3b

Figure 7 Distribution of instantaneous temperature

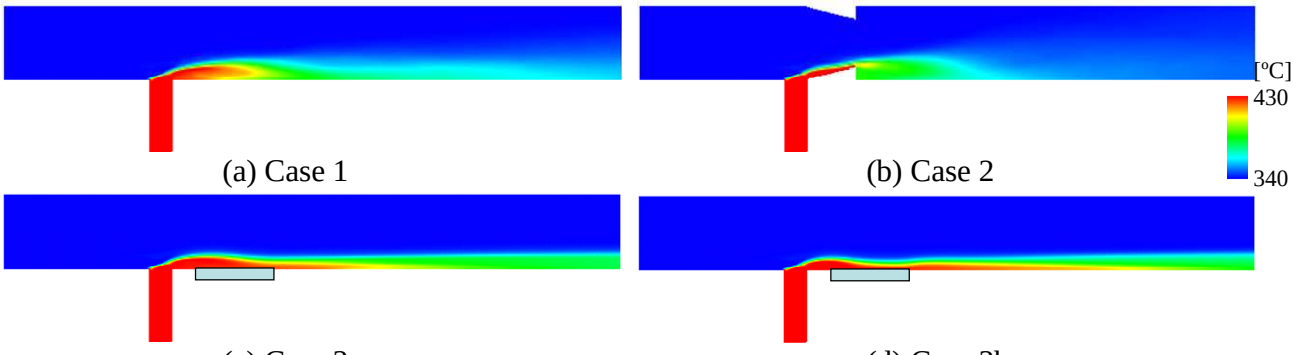

(a) Case 1 (b) Case 2

(c) Case 3a (d) Case 3b

Figure 8 Distribution of average temperature

Figure 9 shows the distribution of the temperature fluctuation (root-mean-square) reduced by the temperature difference ($T'/\Delta T$, ΔT=90ºC). In Case 1 (no additional installation), the maximum temperature fluctuation appears after the junction where a large scale vortex is initiated (see Figure 6(a)) and the comparatively high temperature fluctuation reaches to the bottom of the main pipe as shown in Figure 9(a).

In Case 2 (with turbulence promoter), the high fluctuation region spreads widely in the vertical direction and shortens in the main stream direction after the promoter due to an orifice effect as shown in Figures 9(a) and (b). Hence the maximum value of the fluctuation decreases rather than

that in Case 1, whereas the magnitude of the fluctuation near the bottom wall, in which a thermal fatigue may take place, seems to be similar to that without the turbulence promoter.

When the magnetic field is applied, the fluctuation magnitude decreases considerably as shown in Figures 9(c) and (d). In case with the applied magnetic fields (Case 3a and 3b), there is little discrepancy of the difference between the instantaneous and average temperature distributions as in Figures 7 and 8. Consequently, the temperature fluctuation appears at the interface between the high and low temperatures. It is noted that the magnitude of the fluctuation decreases significantly at the applied magnetic field when the interaction parameter (N) increases.

In a thermal fatigue problem of piping system, it is reported that the temperature distribution along to the radial direction of the pipe is of importance and thus a frequency of the temperature fluctuation near the wall becomes important as well as the magnitude of the fluctuation [8]. When the frequency is low comparing with a characteristic time of radial heat transfer of pipe, no temperature distribution will appear through the radial direction resulting in no thermal fatigue. On the other hand, the heat transfer between the working fluid and the pipe inner surface cannot follow a quite high frequency of the fluctuation resulting also in no thermal fatigue. In a typical piping system of liquid sodium fast reactor, the frequency of approximately several tens Hz would be dominant for the thermal fatigue [8].

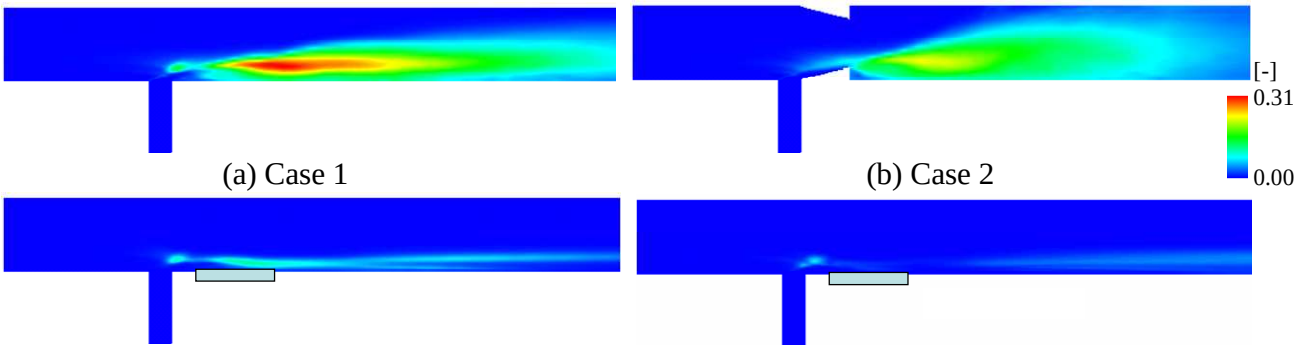

Figure 9 Distribution of temperature fluctuation

Figure 10 shows the auto-power spectrum density (APSD) of the temperature, reduced by the following equation, near the bottom wall where the maximum fluctuation is investigated in Case 1 above (approximately $4D_b$ downstream from junction. see X symbol in the right side of Figure 10).

$$T^* = \frac{T - T_c}{\Delta T} . \tag{19}$$

Here T_c is the temperature of the main flow (T_c = 340ºC).

As shown in Figure 10, the magnitude of APSD near the wall has almost the same both in Case 1 and 2. Although a numerical simulation in three-dimensional is needed to investigate the mixing phenomenon in detail, it might be said that the turbulence promoter has less effectiveness in terms of the fluctuation frequency.

In Case 3a (N=0.55), the magnitude of APSD reduces to approximately one-tenth rather than that in Case 1 or 2, while it almost diminishes in the higher magnetic flux density condition (Case 3b, N=2.10). From the viewpoint of the suppression of thermal fatigue, it is concluded that the interaction parameter (N) will be a good index for design of the applied magnetic field.

With regard to the computational cost, the present analysis with the electromagnetic field (Case 3a and 3b) requires approximately twice as much as that without the electromagnetic field (Case 1 and 2). Since the two-dimensional analysis is carried out in the present study, the computational cost of the modification of the boundary condition of the electric field intensity cannot be estimated reasonably. However, more than 50 subdivided time steps marching are done for the electromagnetic field analysis during one time step of the thermal hydraulics analysis in the present study. It is concluded that a two dimensional thermal hydraulics analysis coupled with an electromagnetic field can be achieved within a reasonable computational cost by using the present method.

As mentioned in 1.2, the iterative manner (matrix solver) is still required at the boundary surfaces in the present method. Therefore, a three-dimensional analysis is necessary to investigate the influence of the matrix solver on the computational cost as well as a comparison between the present method and other coupling methods in existence.

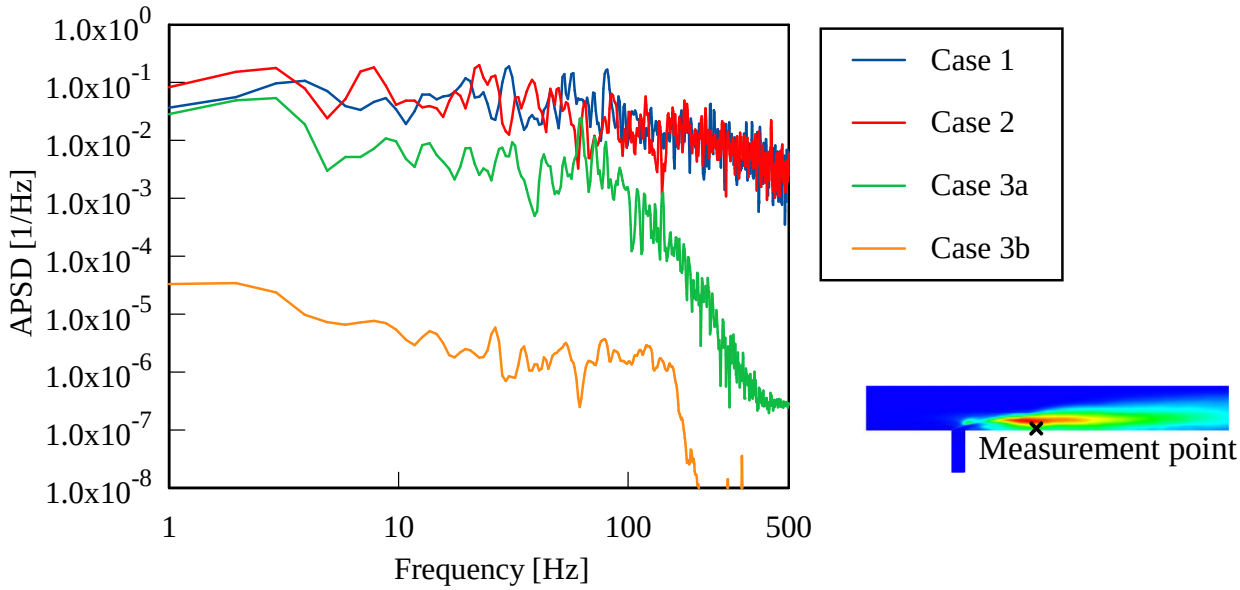

Figure 10 Auto-power spectrum density of reduced temperature

4. Conclusion

A vector finite volume method (VFVM) has been developed to reduce a computational cost. In the VFVM, no iterative manner is required for electromagnetic field in fluid computational domain so as to satisfy the governing equations of the electric filed intensity and magnetic flux density and the solenoidal condition simultaneously. On the other hand, an iterative manner is introduced at boundary surfaces in order to keep a constant magnetic flux density at the boundary during each time step in the computation.

In order to investigate an applicability of the present method and an influence of applied magnetic field on a temperature mixing phenomenon after a T-junction of liquid sodium piping system (thermal fatigue problem), the present method is coupled with the large eddy simulation (LES) of thermal hydraulics and two-dimensional analyses have been carried out for simplicity. In the analyses, an implementation of a turbulence promoter and applied magnetic flux density and its magnitude are chosen as a sensitivity parameter.

As a result, it is demonstrated that the magnitude of the temperature fluctuation decreases by the installation of the turbulence promoter, while the frequency profile of the temperature fluctuation near the wall is less affected by the promoter. On the contrary, the temperature fluctuation decreases significantly when the magnetic flux density is applied after the T-junction due to the Lorentz force. The interaction parameter, which reveals the proportion of the Lorentz force to the inertial force, will be a good index for the suppression of the temperature fluctuation.

With regard to the computational cost, the present method requires twice as much as the thermal hydraulics simulation without the electromagnetic field. In the present analysis, more than 50 subdivided time steps marching are required for electromagnetic field analysis during one time step marching of the thermal hydraulic analysis because of electromagnetic properties in liquid sodium. At least, it can be concluded that the present method is useful for the two dimensional thermal hydraulics analysis coupled with an electromagnetic field analysis. A further investigation will be planned in terms of the computational cost, such as a three dimensional effect and comparison between the other existing methods.

5. References

[1] M. Tanaka, et al., “Thermal Mixing in T-Junction Piping System Related to High-Cycle Thermal Fatigue in Structure”, Journal of Nucl. Sci. and Tech., Vol. 47, No. 9, 2010, pp. 790-801.

[2] M. Igarashi, et al., “Study on Temperature Fluctuation Characteristics for High Cycle Thermal Fatigue in a Mixing Tee”, Transaction of JSME series B, 70, 700, 2004, pp.3150-3157 [in Japanese].

[3] M. Tanaka, et al., “Numerical Simulation of Relaxation Effect by Turbulence Promoter on Temperature Fluctuations”, Proceeding of Annual meeting of Atomic Energy Society of Japan (AESJ), L29, 2006 [in Japanese].

[4] R. Murashige, et al., “Study on Numerical Analysis Method for Electromagnetic Fluid Using Vector Finite Volume Method Consistent with Solenoidal Condition”, Proceeding of the 13th International Topical Meeting on Nuclear Reactor Thermalhydraulics (NURETH13), NURETH13-P1330, Sep. 27- Oct. 2, 2009, Kanazawa, Japan.

[5] R. Murashige, et al., “Numerical Simulation of Electromagnetic Flow Field based on Vector Finite Volume Method”, Proceeding of 7th Korea-Japan Symposium on Nuclear Thermal Hydraulics and Safety (NTHAS7), NTHAS7-N7P0029, Nov. 14-17, 2010, Chuncheon, Korea.

[6] T. Takata, et al., "Application of LES with near wall model in nuclear plant thermal hydraulics", Proceeding of 12th International Topical Meeting on Nuclear Reactor Thermal Hydraulics(NURETH12), 102, Sep. 30- Oct. 4, 2007, Pittsburgh, U. S. A.

[7] Y. Morinishi, et al., "A Study on Wall Boundary Condition in LES", Transaction of JSME series B, 55, 511, 1989, pp. 615-623 [in Japanese].

[8] N. Kasahara, et al., "Structural Response Function Approach for Evaluation of Thermal Striping Phenomena", Nuclear Engineering Design, 212, 2002, pp. 281-292.